Regenerative Therapy 11 (2019) 258–268

Contents lists available at ScienceDirect

Regenerative Therapy

journal homepage: http://www.elsevier.com/locate/reth

Original Article

Intact extracellular matrix component promotes maintenance of liver-specific functions and larger aggregates formation of primary rat hepatocytes

Ronald P. Bual [a, b], Hiroyuki Ijima [a, *]

[a] Department of Chemical Engineering, Faculty of Engineering, Graduate School, Kyushu University, 744 Motooka, Nishi-ku, Fukuoka 819-0395 Japan
[b] Department of Chemical Engineering & Technology, College of Engineering, Mindanao State University-Iligan Institute of Technology, Andres Bonifacio Avenue, Tibanga, 9200 Iligan City, Philippines

ARTICLE INFO

Article history:
Received 26 March 2019
Received in revised form
29 August 2019
Accepted 30 August 2019

Keywords:
Liver-specific extracellular matrix
Hydrogel
Scaffold
Hepatocytes
Tissue engineering

ABSTRACT

The extracellular matrix (ECM) in a liver-specific extracellular matrix (L-ECM) scaffold facilitates hepatocyte viability and maintains hepatocyte functions *in vitro*. However, whether an intact composition of ECM is required for an efficient ECM-based substrate design remains to be clarified. In this study, two L-ECM hydrogels, namely L-ECM I and L-ECM II, were prepared by pepsin solubilization at 4 °C and 25 °C, respectively. The solubility at 4 °C was 50% whereas that at 25 °C was 95%, thus indicating well-preserved L-ECM. Analysis confirmed higher ECM protein components (especially collagen) in L-ECM II, along with denser fiber network and larger fiber diameter. L-ECM II gel exhibited high compression strength and suitable viscoelastic properties. Furthermore, hepatocytes in L-ECM II showed higher expression of liver-specific functions in 3D culture and wider spread while maintaining the cell-cell contacts in 2D culture. Therefore, an intact L-ECM is important to realize effective substrates for liver tissue engineering.

1. Introduction

Extracellular matrix (ECM) is a non-cellular three-dimensional macromolecular network consisting mainly of collagen, elastin, fibronectin, laminins, glycoproteins, proteoglycans (PGs), and glycosaminoglycans (GAGs) [1–3]. These components provide a physical platform for the cells, and stimulate interactive biochemical and biomechanical signals that are required for tissue morphogenesis, differentiation, and homeostasis. Specifically, the ECM facilitates important functions such as binding of growth factors (GFs) and interactions with cell-surface receptors to elicit signal transduction and regulate gene transcription [4]. Thus, natural ECM from native organs has been targeted as engineered scaffolds for tissue engineering in recent years.

Scaffolds composed of natural ECM are typically prepared by decellularization of tissues or organs. Decellularization methods have been extensively studied in the past to optimally retain the native architecture while maintaining the physiological proportions of the ECM components in the tissue [5–8]. The resulting material possesses structural and functional features of the intact organ-specific ECMs along with well-preserved vascular networks [9–11]. L-ECM has been investigated to create functional scaffolds for tissue engineering. The first attempt to produce pepsin-treated L-ECM was reported by Sellaro et al. [12], In their work, L- ECM gels were explored *in vitro*, and maintenance of human hepatocyte functions was confirmed. The versatility of L-ECM was also investigated in two-dimensional (2D) coating and three-dimensional (3D) hydrogel platforms, for the culture and transplantation of primary hepatocytes, as reported by Lee et al. [13]. Their results indicated significantly improved hepatocyte functions both *in vitro* and in vivo. Despite these successful attempts and current efforts in the application of L-ECM, there is still much work to be done to identify the signaling mechanisms that promoted improved hepatocyte function on L-ECM. Thus, a deeper understanding of its nature and how protein component works will help create optimal design of L-ECM substrates for in-vitro liver tissue engineering.

In our previous studies, the physical properties of L-ECM from porcine liver [11] and a hepatocyte growth factor (HGF)-

* Corresponding author. Fax: +81 92 802 2748.
E-mail address: ijima@chem-eng.kyushu-u.ac.jp (H. Ijima).
Peer review under responsibility of the Japanese Society for Regenerative Medicine.

https://doi.org/10.1016/j.reth.2019.08.006

immobilized L-ECM scaffold for hepatocyte culture were reported [14]. Also, a L-ECM nanofiber was fabricated for use as substrate to primary rat hepatocytes [15]. However, the solubility of L-ECM, using our established protocol, was only about 50%, which implies that 50% of the L-ECM was left undissolved. Since the behavior of cells is influenced by the components and structure of the ECM [16], it is crucial to determine how the changes in specific protein components affect the stability of ECM-based scaffold and influence liver-specific phenotypes of hepatocytes.

In this study, pepsin-solubilized L-ECM was prepared by a different protocol. The chemical and physical properties were evaluated thereafter, and two- and three-dimensional cultures, using primary hepatocytes, were performed to investigate its effectiveness. The behavior of hepatocytes *in vitro* (e.g., morphology and function) was expected to be affected by the components and structure of L-ECM.

2. Methods

2.1. Decellularization and solubilization of porcine liver

2.1.1. Decellularization

Decellularization was performed as described previously [14]. Briefly, a healthy porcine liver was harvested from adult pig (20–25 kg) (Fukuokashokunikuhanbai Co., Ltd., Fukuoka, Japan) and depleted of blood with calcium and magnesium-free phosphate-buffered saline (CMF-PBS). The liver was cut into 1 cm × 1 cm × 2 mm pieces using a mandoline-style slicer. The sliced tissue was soaked in a solution containing 1% Triton X-100 (Wako Pure Chemical Industries, Ltd., Osaka, Japan) in CMF-PBS at 4 °C for 3 days to remove the cellular components. Fresh solution was added each day, for 3 days, under constant stirring to maintain the efficiency of decellularization. The resulting decellularized liver was immersed in CMF-PBS at 4 °C for 4 days, and then dialyzed using the Spectra/Por 6 dialysis membrane (MWCO: 1000 kD, Spectrum Laboratories, Inc., Milpitas, CA, USA) at 4 °C for 2 days.

2.1.2. Solubilization and preparation of L-ECM hydrogel

The decellularized liver was lyophilized for 24 h to obtain dried porcine L-ECM. The lyophilized L-ECM was then milled using a mill mixer. In method I, 100 mg of the L-ECM powder was measured and mixed with 10 mg pepsin (Sigma–Aldrich, St. Louis, MO, USA) in 10 mL of 0.1 N HCl. The mixture was constantly stirred for 3 days at 4 °C. In method II, 100 mg of L-ECM powder was mixed with 10 mg pepsin in 10 mL of 0.01 N HCl. The mixture was constantly stirred for 2 days at room temperature (approximately 25 °C). The samples produced by methods I and II were referred to as L-ECM I and L-ECM II, respectively. Once the L-ECM sol was produced, dialysis was performed at 4 °C for 1 day. The subsequent viscous solution of solubilized L-ECM (pH = 3.0–4.0) was mixed with concentrated Eagle's minimum essential medium (MEM) (10×) and buffer (47.7 mg HEPES/mL, 0.08 N NaOH), at a volume ratio of 8:1:1 (*v*/*v*), and kept on ice. The solution formed a gel, after incubation at 37 °C for 30 min, by assembling itself into a three-dimensional network.

2.2. Biochemical analysis of solubilized L-ECM

2.2.1. Analysis of total protein content

The amount of protein in the L-ECM digests was quantified using the Pierce BCA Protein Assay kit (Thermo Fisher Scientific, Waltham, MA, USA), and absorbance at 540 nm was recorded using a microplate reader (Perkin Elmer, Waltham, MA, USA).

2.2.2. Analysis of collagen content

Collagen content was measured using a collagen quantitation kit (Cosmo Bio Co., Ltd., Tokyo, Japan) according to the manufacturer's protocol. This kit is highly specific and sensitive for assaying whole collagen in biological samples using a fluorogenic reagent, 3,4-dihydroxyphenylacetic acid (3,4-DHPAA). The 3,4-DHPAA reagent can selectively detect N-terminal Gly-containing peptides and estimate the accurate amount of collagen in a biological sample. A fluorescence plate reader (1420 ARVOMX-L2 system: Perkin Elmer, MA, USA), set at a wavelength of 465 nm, was used in this study.

2.2.3. Evaluation of sulfated glycosaminoglycan

Sulfated glycosaminoglycan (GAG) content was selected as an indicator of alterations in the structural composition of the decellularized tissue. The sulfated GAG content of L-ECM digest was assessed by recording the absorbance at 620 nm using the Alcian Blue 8GX assay (Sigma–Aldrich). The concentration of GAG was calculated using a standard curve of heparin sodium in water (12.5–400 μg/mL). The results were expressed as micrograms per milligram of wet tissue weight.

2.2.4. Analysis of molecular weight distribution of proteins

Sodium dodecyl sulfate polyacrylamide gel electrophoresis (SDS-PAGE) (AE-6500, ATTO Corporation, Tokyo, Japan) was performed for the determination of molecular weight distributions. L-ECM samples, at 10 mg/mL and 5 mg/mL, and acid-solubilized porcine type I collagen (referred as I Col) (Nitta Gelatin Inc., Osaka, Japan) were prepared. A 5% acrylamide gel was used, and each sample was electrophoresed at 200 V and 20 mA for 1 h according to the manufacturer's instructions.

2.3. Scanning electron microscopy

L-ECM and I Col (3 mg/mL) samples were adjusted to neutral pH with reconstitution buffer (47.7 mg HEPES/mL, 0.08 N NaOH) and 10× MEM at a ratio of 8:1:1. Each adjusted sample concentration was four-fifths of the above concentration. The solution formed a gel, after incubation at 37 °C for 30 min, by assembling itself into a three-dimensional network. The sample was then dehydrated in the presence of ethanol and t-butanol (Wako). After which, the hydrogel was allowed to stand at 4 °C, and was dried using a freeze-dryer. Morphological structure of the obtained dried sample was observed under a scanning electron microscope (SEM, SU3500, Hitachi High-Technologies Corporation, Tokyo, Japan). Prior to SEM, the samples were pretreated using osmium coater (HPC-ISW, Vacuum Device Inc., Japan).

2.4. Rheology of gels

In order to investigate the gelation behavior of L-ECM, rheological evaluation was performed. Samples of L-ECM and I Col were adjusted to neutral pH by mixing with reconstitution buffer and 10× MEM at a ratio of 8:1:1. Analysis of rheological properties was conducted using a rheometer (MCR 302, Anton Paar, Japan). A parallel plate of 25-mm diameter and a cone plate of 25-mm diameter were used for the measurement of frequency sweep and strain sweep, respectively. The storage modulus (G′, elastic term) and loss modulus (G″, viscous term) were determined and expressed as graphs with respect to distortion and frequency.

2.5. Compression of gels

L-ECM and I Col (3 mg/mL) samples were adjusted to neutral pH by mixing with reconstitution buffer (47.7 mg HEPES/mL, 0.08 N NaOH) and 10× MEM at a ratio of 8:1:1. Thereafter, 500 μL were

placed in a 24-well plate and incubated at 37 °C for at least 30 min. Stress due to compression of the gel was measured using a load measuring machine (LTS-50N-S100: Minebea Co., Nagano, Japan). Height of the gel was measured, and a stress-strain curve was generated.

2.6. Degradation of gels

L-ECM samples from methods I and II, or 3 mg/mL I Col were adjusted to neutral pH with reconstitution buffer and 10× MEM at a ratio of 8:1:1. Each adjusted sample concentration was equal to four-fifths of the above concentration.

For *in-vitro* degradation test, collagenase digestion was performed. A gel volume of 500 μL was shaken in 10 mL of 0.5 mg/mL collagenase (Wako)/0.05 mg/mL trypsin inhibitor (Wako) solution mixture, and weight of the gel was measured at a predetermined time interval. After weighing, fresh medium was added for the next time interval. The extent of degradation was calculated using the following equation:

$$Weight\ \ Change(\%) = W_f \Big/ W_i \times 100$$

where W_f is the weight of the hydrogel at a given time, and W_i is the initial weight of the hydrogel.

2.7. In-vitro studies of L-ECM gels

2.7.1. Isolation and inoculation of primary rat hepatocytes

Primary hepatocytes were isolated from 6–8-week-old male SD rats (Japan SLC, Inc., Hamamatsu, Japan). Hepatocytes were prepared using a two-step collagenase perfusion method [17], and cell viability was found to be approximately 92% using Trypan blue exclusion test. The culture medium consisted of Dulbecco's Modified Eagle's medium (DMEM), supplemented with 10 mg/L insulin from bovine pancreas (Sigma), 7.5 mg/L hydrocortisone (Sigma), and 60 mg/L L-proline (Sigma); it was hence named as D-HDM [14,18]. This protocol was reviewed and approved by the Ethics Committee on Animal Experiments of Kyushu University (A29-413-1, 29 Jun 2018).

Before hepatocyte culture, L-ECM pre-gels were adjusted to neutral pH with reconstitution buffer and 10× MEM at a ratio of 8:1:1. Each adjusted sample concentration was equal to four-fifths of their original concentration. Then, freshly isolated hepatocytes were seeded onto L-ECM pre-gels at a seeding density of 2.5×10^5 cells/mL. By incubation under standard conditions (37 °C, 5% CO_2, 95% air) for at least 30 min, hepatocyte-seeded L-ECM gels were obtained. Finally, two hundred microliters of D-HDM was added to each well of a 48-well cell culture plate. The culture medium was refreshed after 1, 3, 5, and 7 days. At least three independent hepatocyte culture experiments were conducted to check the reliability of the results.

2.7.2. Expression of liver-specific functions in hepatocytes

Albumin concentration in the culture medium was measured using the protein detector ELISA kit HRP/ABTS system (Kirkegaard & Perry Laboratories, Gaithersburg, MD, USA). Rat albumin standard and anti-rat albumin antibody were purchased from ICN Pharmaceuticals (Aurora, OH, USA).

Meanwhile, the ammonia metabolism was estimated by measuring ammonia concentration in the medium. Briefly, the medium was substituted with 1 mM ammonium chloride-supplemented D-HDM and incubated for 3 h. Ammonia metabolism was measured using the ammonia test (Wako Pure Chemical Industries) using the manufacturers protocol.

Ethoxyresorufin-O-deethylase (EROD) activity, an indicator of CYP1A1 (Cytochrome P450 family 1 subfamily A member 1) activity, was estimated by measuring the intensity of resorufin fluorescence in the medium. In this assay, CYP1A1 was induced by 3-methylcholanthrene (Sigma). Briefly, the medium was substituted by 4 mM 3-methylcholanthrene (Sigma)-supplemented D-HDM and incubated for 24 h. After that, the medium was replaced with 20 mM ethoxyresorufin (Wako Pure Chemical Industries)-supplemented D-HDM and incubated for 2 h. The intensity of resorufin fluorescence in the medium was measured using a fluorescence plate reader.

Furthermore, Cell Counting Kit − 8 (CCK-8, Dojindo Molecular Technologies, Inc., Rockville, MD, USA) was employed for the approximation of viable cell number. CCK-8 allows very convenient assays by utilizing Dojindo's highly water-soluble tetrazolium (WST) salt. WST-8 [2-(2-methoxy-4-nitrophenyl)-3-(4-nitrophenyl)- 5-(2,4-disulfophenyl)-2H-tetrazolium, monosodium salt] produces a water-soluble formazan dye upon reduction in the presence of an electron mediator. The amount of formazan dye after 2-h incubation (measured by absorbance at 450 nm) is directly proportional to the number of viable cells.

The results obtained for albumin concentration, ammonia metabolism, and EROD activity were divided by WST-8 as an index of liver function per viable cell number.

2.8. Preparation and morphology evaluation of hepatocyte-cultured L-ECM films

L-ECM films were prepared as described in a previous report [14]. Briefly, 0.03 mg/mL solution of L-ECM was prepared using sterile water, and 200 mL/well was added to a 48-well cell culture plate (bottom area: 1.1 cm^2, product no. CN-150687, Thermo Fisher Scientific, Kanagawa, Japan). The solution was air-dried on a clean bench for approximately 2 days, after which, the film was cross-linked with 1% glutaraldehyde (Wako) for 3 h for stabilization. Residual glutaraldehyde was removed by washing with CMF-PBS. Finally, the film was washed with basal medium (DMEM) to inactivate any residual glutaraldehyde. Films of collagen (Cellmatrix Type I-C: 3 mg/mL; Nitta Gelatin, Osaka, Japan) were also prepared using the same method.

Freshly isolated hepatocytes were inoculated onto L-ECM films under standard conditions (37 °C, 5% CO_2, 95% air) at a seeding density of 2.5×10^4 cells/mL. Two hundred microliters of D-HDM was added to each well of a 48-well cell culture plate. The culture medium was changed after 1, 3, 5, and 7 days. During the 7-day culture, morphology of the hepatocytes was studied using a cell culture microscope (Olympus CKX53, Nagano, Japan).

2.9. Statistical analysis

All calculated values are presented as the mean ± standard deviation. Statistical analysis of the data was performed using one-way ANOVA for simple 3 groups and two-way ANOVA for time-dependent 3 groups. A p-value < 0.05 was considered statistically significant.

3. Results

3.1. Solubility of L-ECM powder in pepsin solution

The solubility of L-ECM powder in pepsin-HCl solution was tested using two methods (Fig. 1). In method I (Fig. 1a), insolubilized L-ECM powder was observed compared to that in method II, in which it was almost homogeneous (Fig. 1b). These observations

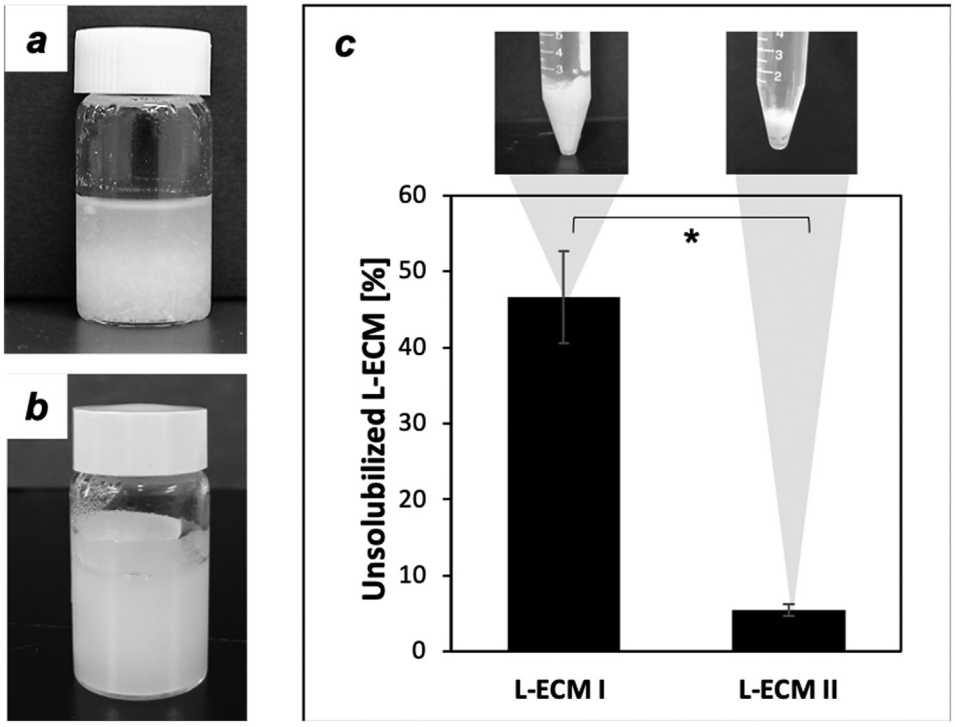

Fig. 1. Pepsin solubilized L-ECM. *(a)* L-ECM produced using method I, *(b)* L-ECM produced using method II, and *(c)* Percentage of insolubilized L-ECM. n = 3. Bars represent standard deviation. $^{*}p < 0.05$).

were confirmed, as seen in Fig. 1c, after weighing the lyophilized insoluble L-ECM solids.

3.2. Component evaluation in solubilized L-ECM

The protein content of L-ECM II was much higher than that of L-ECM I (Fig. 2a); in L-ECM II, the total protein content was 6262 ± 463 μg/mL, indicating a 43% difference. This result was further confirmed in Fig. 2b, since L-ECM II contained 3215 ± 77 μg/mL collagen, which was 61% higher than in L-ECM I. However, L-ECM I had slightly higher concentration of GAGs, as shown in Fig. 2c. This finding confirmed that GAGs may be well-preserved at 4 °C than at room temperature pepsin solubilization.

The bands in SDS-PAGE, representing the molecular weight distribution of pepsin-solubilized ECM, were studied next (Fig. 3). Differences in relative intensities of the molecular weight bands were confirmed. The noticeable bands occurring around 220 kDa, 210 kDa, and 120 kDa indicated collagen molecule γ, β, and α chains, respectively. The α_1 and α_2 chains were found to be the major constituents that form the triple helical structure of collagen molecules. Specifically, L-ECM II had a more intense band for α chains (indicated by deep purple color) than L-ECM I.

3.3. Scanning electron microscopy of lyophilized gels

The SEM photos in Fig. 4 were obtained by dehydration of hydrogels. Thus, they may not necessarily imply the state of ECM in the actual hydrogel. However, these images are indispensable to deduce the skeleton structure of ECM gel. Based on Fig. 4a–f, fibrous skeleton was observed in all samples. Comparing these images, fiber densities were found to be higher in L-ECM gels (Fig. 4b, e, c, f) than in I Col gel (Fig. 4a, d), resembling a mesh-like structure. In addition, the highest average fiber diameter (Fig. 4g) was in L-ECM II gel and lowest in I Col gel with 129.8 ± 4.4 nm and 41.4 ± 6.1 nm, respectively. Based on these results, the fiber diameter and fiber density were deduced to be dependent on the constituent components.

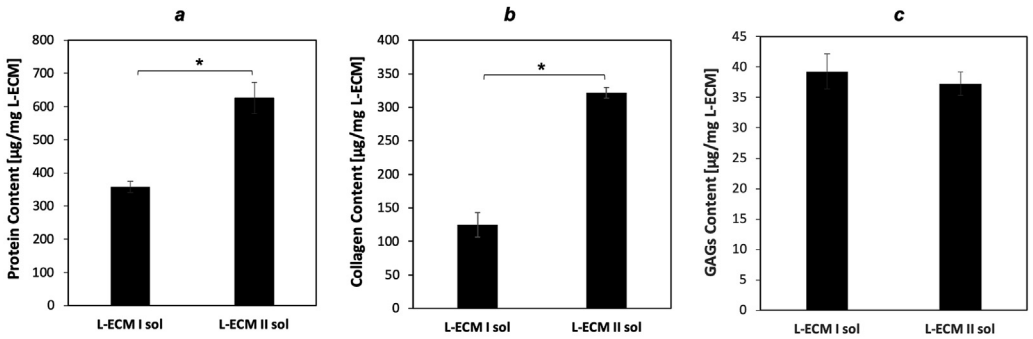

Fig. 2. Biochemical components in the solubilized L-ECM. *(a)* Total protein, *(b)* collagen, and *(c)* GAG concentrations. n = 3. Bars represent standard deviation. $^{*}p < 0.05$.

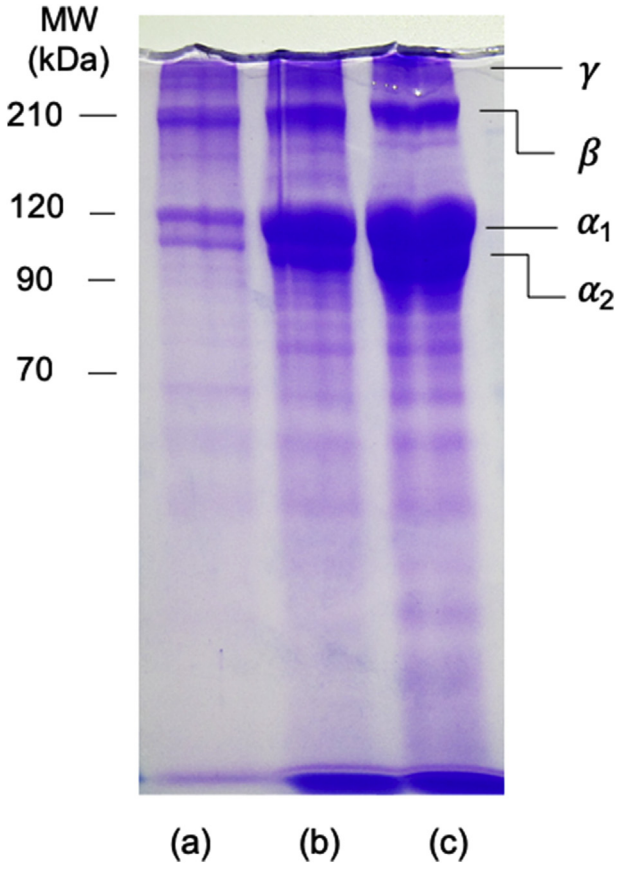

Fig. 3. SDS-PAGE analysis of (a) I Col, (b) L-ECM I, and (c) L-ECM II.

3.4. Rheology of hydrogels

The rheograms in Fig. 5a show similar profiles of storage modulus under all conditions. Moreover, the storage moduli were greater than the loss moduli ($G' > G''$). L-ECM gels had higher viscoelasticity than I Col hydrogel, owing to the presence of components other than collagen. In the initial frequency stage of L-ECM II hydrogel, at 1–10 s^{-1} frequency range, the storage modulus was maintained at approximately 101 Pa and then gradually increased up to 200 Pa at the end of the frequency sweep mode test. At increased frequencies, a non-linear behavior was observed in both G′ and G′′. On the other hand, the rheograms in Fig. 5b show non-linear profile of G′ and G″ under all conditions. Similar to that in Fig. 5a, the viscoelastic profile of L-ECM II hydrogel for both G′ and G″ was better than in other samples. In L-ECM II hydrogel, G′ was maintained at 297 Pa at 1–2% strain, and gradually decreased to 130 Pa at the end of strain sweep test.

3.5. Compression test for gels

Compression stress was detected in all samples, as shown in Fig. 6. The highest stress was obtained in L-ECM II gel, followed by L-ECM I gel, and the lowest was I Col gel with 5.1 ± 1.3 kPa, 4.3 ± 0.5 kPa, and 3.5 ± 0.8 kPa, respectively. The difference in mechanical behaviors is a manifestation of the unique internal fiber network structures of the hydrogel samples.

3.6. Gel degradation analysis

Here, we investigated the degradation of hydrogels in the presence of collagenase and confirmed the reduction in weight over time (Fig. 7). At the initial time point (20–30 min), the changes in weight of I Col, L-ECM I, and L-ECM II hydrogels were 52.1 ± 0.6%, 80.8 ± 0.9%, and 82.5 ± 1.4%, respectively. The I Col gel completely degraded after 150 min, L-ECM I gel degraded after 180 min, and L-ECM II gel degraded after 260 min.

3.7. Functional evaluation of hydrogels using primary hepatocytes

The morphological features, observed under a phase-contrast microscope, showed the phenotypic changes of hepatocytes (Fig. 8). During day 1 of the culture, hepatocytes started to form clusters with their adjacent cells and the difference in their morphology across the scaffolds was minimal (Fig. 8, 1st column). After days 3–7 of culture, hepatocytes formed bigger clusters, producing a more recognizable morphology between scaffolds (Fig. 8, 2nd – 4th column). While it was difficult to deduce any difference in morphology after day 7, hepatocytes were seen able to form tissue-like morphologies under 3D culture conditions.

Changes in phenotype during the 7-day culture were evaluated by determining the relative expression of liver-specific functions such as EROD activity, WST-8 activity, ammonia secretion rate, and albumin production. As shown in Fig. 9a, EROD activity decreased from day 3 to day 5 and then remained steady until day 7 under all conditions. In I Col gel, EROD activity showed a huge decrease at day 5 compared to that in L-ECM gels. Specifically, higher function was observed in L-ECM II gel, with relative intensity equal to

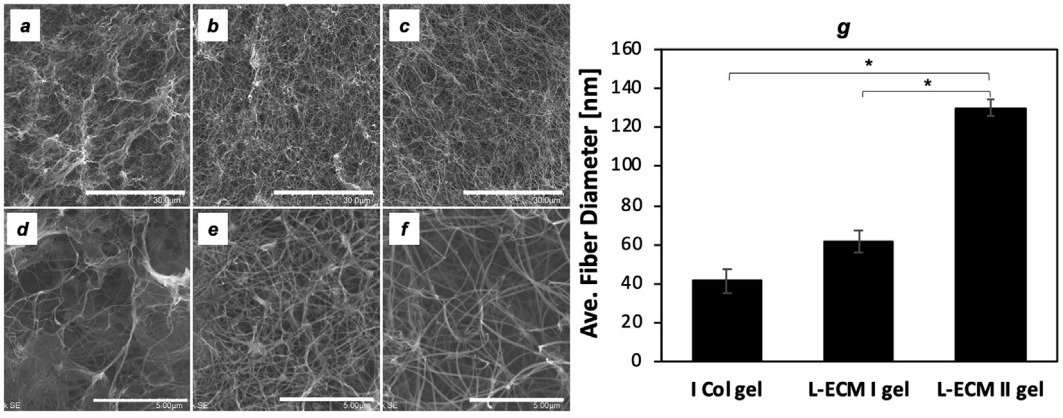

Fig. 4. Scanning electron microscopy of lyophilized hydrogel. *a, d)* I Col gel, *b, e)* L-ECM I gel, and *c, f)* L-ECM II gel (For low magnification *(a – c)*, scale bars = 30 μm, for high magnification *(d – f)*, scale bars = 5 μm), and *g)* Average diameter of the fibrous network in hydrogels (n = 3). Bars represent standard deviation. $^{*}p < 0.05$.

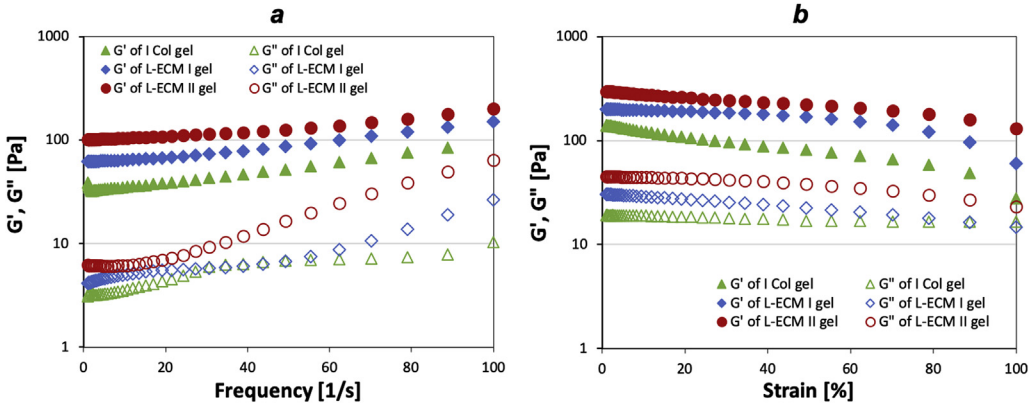

Fig. 5. Rheological properties of hydrogels. *a)* Frequency sweep mode measured from 1 to 100 rad/s, with a strain of 1%, at a temperature of 24 °C (n = 3). *b)* Strain sweep mode measured from 1 to 100% with a constant frequency of 10 rad/s at a temperature of 24 °C (n = 3).

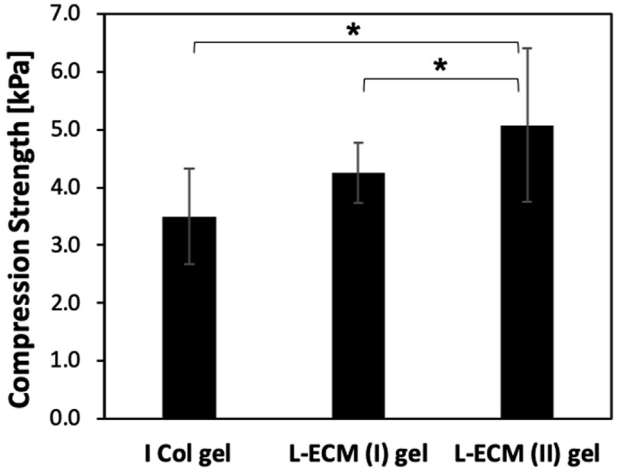

Fig. 6. Mechanical property of hydrogels (n = 3). Bars represent standard deviation. $^{*}p < 0.05$.

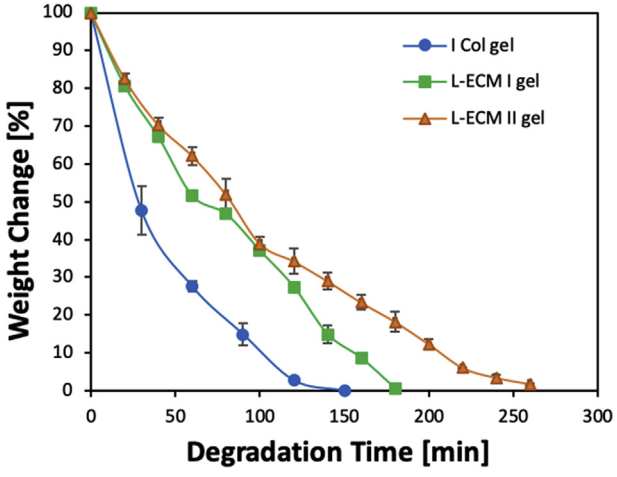

Fig. 7. Degradation profile of hydrogel. Bars represent standard deviation (n = 3).

1137 ± 51 at the end of day 7. This intensity was 11% and 44% higher than in L-ECM I and I Col gels, respectively. On the other hand, as shown in Fig. 9b, the index of viable cell number increased as gels got degraded over time. In I Col gel, the number of viable cells was 33% and 46% higher than in L-ECM I and L-ECM II gels at day 7 of culture. This might be explained by the faster degradation of I Col gel, resulting in the appearance of viable hepatocytes. However, the functional ability of cells depends on the microenvironment of the hydrogel and thus, determining the function per viable cell is an important parameter to consider. In Fig. 9c, all conditions showed reduced function per viable cell during the 7-day culture. Here, L-ECM gels showed gradual decreased in liver function in contrast to I Col gel. Consistently, L-ECM II gel showed higher function per viable cell at the end of day 7, which was 29% and 70% higher than that of L-ECM I and I Col gels, respectively.

The albumin secretion rate was monitored using ELISA detection system during the 7-day culture. As shown in Fig. 10a, the albumin secretion rate, in most of the conditions, decreased over time. However, higher secretion rate was manifested in L-ECM II gel (16.6 ± 0.8 μg/mL at day 3, 13.4 ± 0.8 μg/mL at day 5, and 10.9 ± 0.4 μg/mL at day 7) relative to that in L-ECM I and I Col gels. The albumin secretion rate per viable cell number showed a similar profile (Fig. 10b) as in Fig. 10a. Specifically, the L-ECM II gel showed 65.9 ± 3.3 μg/mL/viable cell at day 3, which was 41% higher than that in L-ECM I and 80% higher than in I Col gel. Even during day 7, the function remained higher in L-ECM II gel, with 33.7 ± 0.9 μg/mL/viable cell compared to 15.4 ± 1.0 μg/mL/viable cell and 4.5 ± 0.2 μg/mL/viable cell in L-ECM I gel and I Col gel, respectively.

Ammonia metabolism is a characteristic function of a mature differentiated liver. In Fig. 10c, the ammonia metabolism rates are shown, and in Fig. 10d, the metabolism rate per viable cell is shown. In both figures, the ammonia metabolism decreased over time. Nevertheless, L-ECM II gel showed higher function per viable cell than L-ECM I and I Col gels during the 7-day culture.

The morphology of hepatocytes was studied in 2D cultures to distinguish between the hydrogel samples (Fig. 11). Noticeable differences were observed in each sample during the 7 days of culture. In I Col film, hepatocytes did not spread on the surface, in contrast to that in L-ECM films (Fig. 11a); hepatocytes were well spread while maintaining cell-cell contact on the surface of the L-ECM films (Fig. 11b–c). Using ImageJ software, area of the largest hepatocyte aggregates divided by the total area of the specimen (as seen on the microscope image) was calculated to determine the index of hepatocyte spreading. The areas of the largest hepatocyte aggregates at day 3 were 11,885 μm^2 and 21,256 μm^2 for L-ECM I and L-ECM II, respectively. These spreading areas accounted for approximately 22.1% in L-ECM I and 39.5% in L-ECM II (Fig. 11b–c, 2nd column). At day 5, the spread increased to 42.6% in L-ECM I and 75.2% in L-ECM II (Fig. 11b–c, 3rd column). At the end of day 7, L-ECM II film (Fig. 11c, 4th column) produced a wider hepatocyte

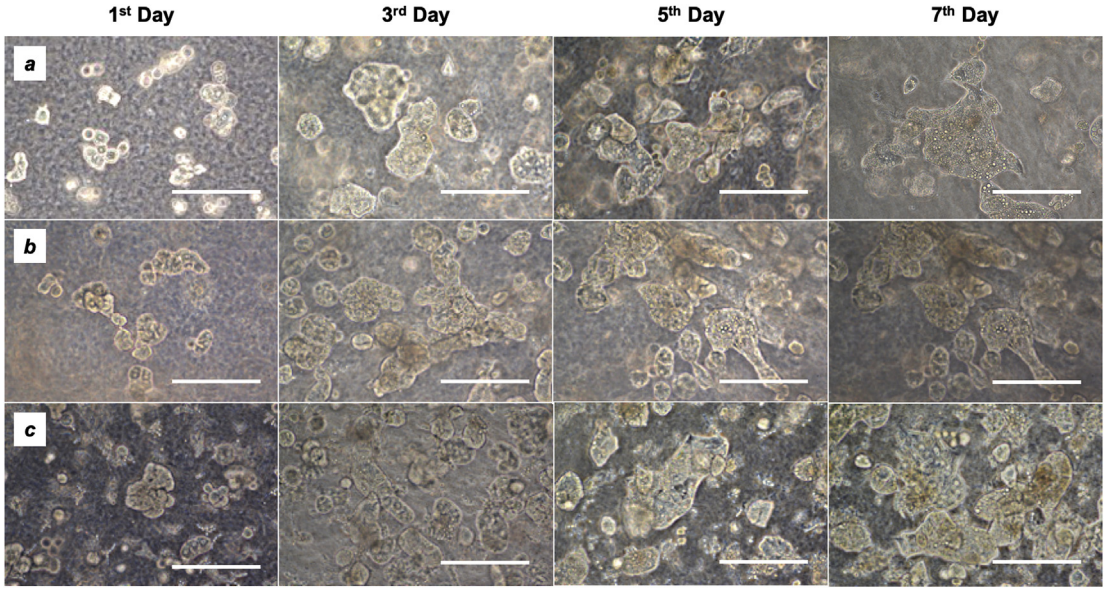

Fig. 8. Morphology of hepatocytes in 3D culture after 1, 3, 5, and 7 days, under phase-contrast microscope. *a)* I Col gel, *b)* L-ECM I gel, and *c)* L-ECM II gel (scale bars = 100 μm, magnification = 20×).

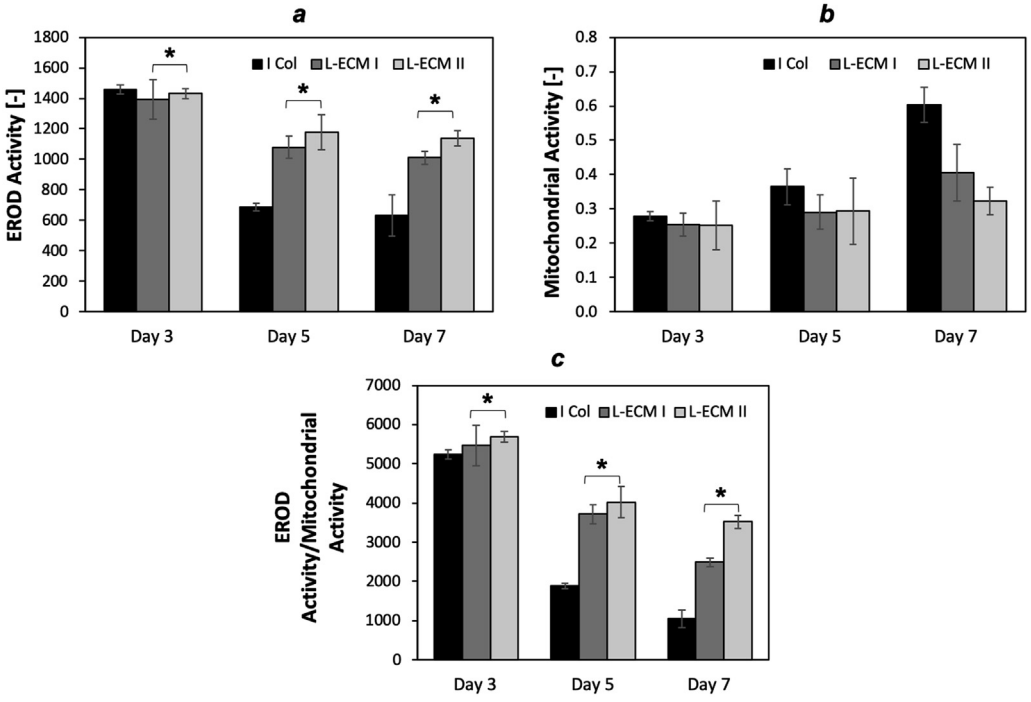

Fig. 9. Relative expression of hepatocyte functions: *a)* EROD activity, *b)* mitochondrial activity, and *c)* EROD activity per mitochondrial activity (index of CYP1A1 enzyme activity per viable cell) after 3, 5, and 7 days of culture on hydrogels. n = 3. Bars represent standard deviation. $^{*}p < 0.05$.

spread area (at 79.0%) compared to the 58.5% in L-ECM I (Figure 11b, 4th column).

4. Discussion

The challenge of maintaining hepatocyte phenotype *in vitro* has led to the development and application of tissue-specific ECM substrates. Recreating a natural microenvironment in culture allows hepatocytes to function and interact as they would in normal healthy liver tissue. Several studies have demonstrated the advantages of culturing hepatocytes on natural, tissue-specific ECM substrates compared to that on purely synthetic substrates [12,14,19–21]. Although the underlying mechanisms for this improved phenotypic stability are still unknown, they are likely related to the inclusion of several components of the natural liver microenvironment.

The solubilization protocol at room temperature maximized the activity of pepsin, thereby increasing the solubility of L-ECM. The resulting L-ECM sol (L-ECM II) is composed of high ECM protein components such as collagen and GAGs. Although the amount of

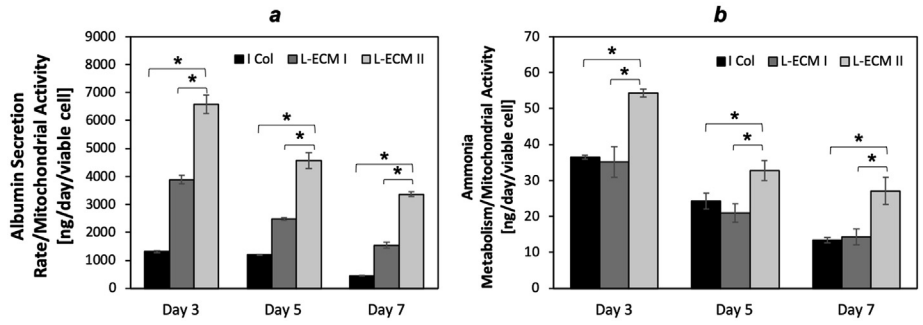

Fig. 10. Expression of hepatocyte functions: *a)* albumin secretion rate per mitochondrial activity (index of albumin secretion rate per viable cell), *b)* ammonia metabolism rate per mitochondrial activity (index of ammonia metabolism per viable cell) after 3, 5, and 7 days of culture on hydrogels. n = 3. Bars represent standard deviation. $^{*}p < 0.05$.

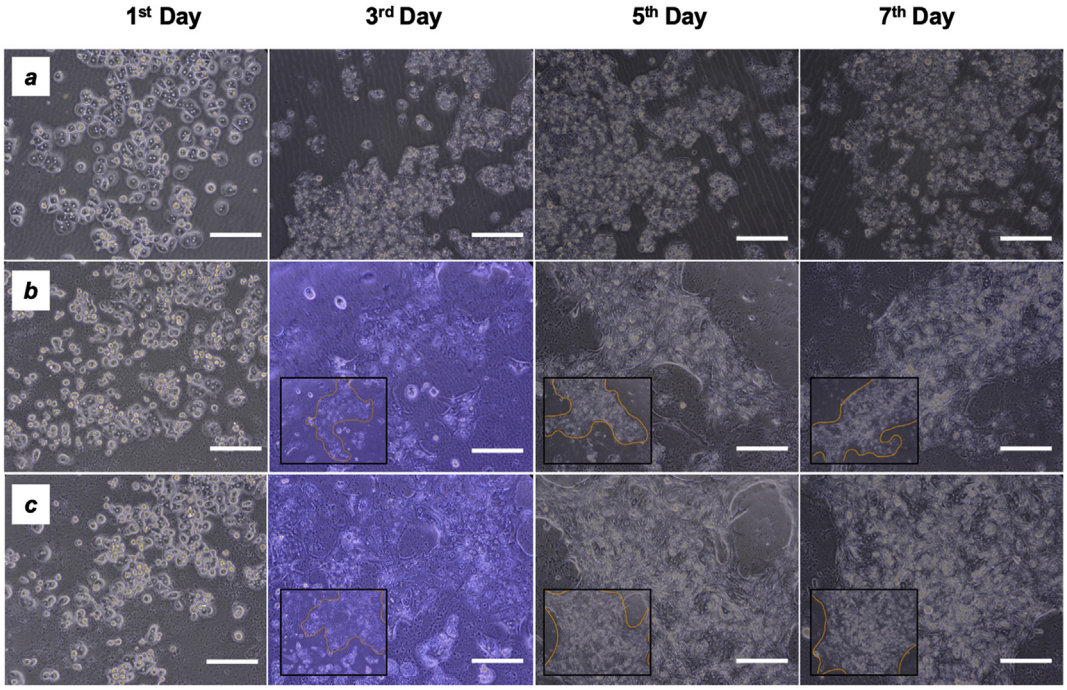

Fig. 11. Morphology of hepatocytes in 2D culture after 1, 3, 5, and 7 days under phase-contrast microscope. *a)* I Col film, *b)* L-ECM I film, and *c)* L-ECM II film (scale bars = 100 μm, magnification = 20×).

other ECM components (e.g., laminin, fibronectin, and elastin) might also be changed, it would need further validation before discussion. Pepsin solubilization cleaved the cross-link containing telopeptide, and the β-chain was concurrently cleaved into two α-chains [22]. The α_1 and α_2 chain patterns were similar to that of standard collagen Type I which suggested that Type I collagen is the major component in the L-ECM sol. Correspondingly, this observation agrees with the findings reported previously [11,23,24]. Moreover, the presence of higher protein concentration (esp. collagen) manifested in a higher-density mesh-like structure and larger fiber diameters in L-ECM II gel.

Mechanical properties of tissue microenvironments contribute to the overall functioning and health of the organ systems they comprise. In the liver, many forces exist, including compression, tensile strength, shear stress induced by fluid flow in the vasculature, and other types of forces applied by cells in the matrix [25,26]. These forces affect multiple aspects of cell function, including differentiation, growth and survival, and adhesion [27,28]. Substrates should be designed to withstand the specific biomechanical needs of hepatocytes. In this study, results confirmed that the increased amount of proteins relatively increased the compression strength and viscoelastic property of L-ECM II hydrogel. Since collagen is the main component in the ECM [29], it is the main dictator of the structure and function of the ECM. Our results also demonstrated that the collagen structures reconstituted in L-ECM hydrogels may be very similar to the native nanofiber collagen architecture. Thus, L-ECM II gel may provide adequate biomechanical strength to support hepatocytes, compared to L-ECM I and I Col hydrogels.

Control of the degradation rate is also important to support cellular activities (e.g. proliferation and migration) during tissue remodeling [26,30]. Additionally, biodegradability of hydrogels is vital to ensure safety for clinical use and avoid potential toxicity. Naturally, ECM is degraded in presence of type II collagenase, a member of the matrix metalloprotease family, which then degrades the extracellular matrix and promotes cell migration and growth [26]. Results showed that rate of degradation was the lowest in L-ECM II hydrogel, which was attributed to its improved biomechanical and viscoelastic strength. For liver transplantation, this phenomenon is important to provide sufficient time for the hydrogel scaffold to develop a new tissue-like structure, prior to

complete degradation. Three fundamental mechanisms of degradation have been suggested for hydrogels: hydrolysis, enzymatic cleavage, and dissolution [31–33].

The interaction between cells and ECM regulates important cellular behavior and functions. In most cases, a well-designed 3D cell culture system can recapitulate complex *in-vivo* physiological constructions and tissue microenvironments, thereby serving as a better model than a conventional 2D cell culture [19,34]. In this report, morphology of the cells was studied using phase-contrast microscope to distinctly understand the phenotypic changes across hydrogel samples. Though hepatocytes developed into large aggregates or organoids during the 7-day culture under all conditions, significant difference was not visible. Since tissue-like cell aggregates formed in different directions inside the hydrogel, they were difficult to compare microscopically. Tissue-like structures, formed by the aggregation of primary hepatocytes in culture, can prevent dedifferentiation [35], and thus stimulate manifestation of liver-specific functions.

In 2D culture, difference in morphology was noticeable under all conditions. Clearly, in I Col film, hepatocytes did not produce clusters during the 7-day culture, in contrast to that in L-ECM films. Comparing the hepatocyte clusters in the L-ECM films, L-ECM II was found to produce the widest spread area and formation of tissue-like structure at the end of day 7. This result may indicate the presence of suitable mechanical properties and intact ECM components in the L-ECM II. In 3D culture, hepatocytes exhibited better expression of liver-specific functions such as EROD activity, albumin synthesis, and ammonia metabolism in L-ECM hydrogel than in I Col hydrogel during the 7 days of culture. Therefore, the intact ECM components stimulated sustained release of functional molecules, as a result of which, abundant liver-specific signals were transmitted to the surrounding cells and triggered site-specific differentiation of hepatocytes.

The relative increase of mitochondrial activity in I Col hydrogel may indicate the appearance of cells on the surface as it undergoes biodegradation. Therefore, when the hydrogel structure collapsed, cells may have resurfaced, and promoted signal on WST-8. Though diffusion of cell-related signals might possibly occur within the hydrogel, it may be smaller compared to when the cell is directly in contact with the medium. The slower degradation rate of L-ECM II gel resulted in a steady and minimal increase of mitochondrial activity signal with respect to culture time. In other words, a mechanically stable hydrogel facilitated the controlled released of bioactive substances [33]. The ideal condition is that the rate of scaffold degradation should mirror the rate of new tissue formation or be adequate for the controlled release of bioactive molecules [33]. However, the effects of ECM degradation on cell behavior are possibly more complex due to the combination of changes in the nature of physical interactions between the cell and degraded ECM proteins, and the release of a host of ECM-sequestered cytokines [36].

Based on a study by Rubin et al., the rate of hepatocyte spreading was seen to be increased with the amount of collagen molecules in the substrate [37]. Since the content of solubilized collagen was higher in L-ECM II, it not only promoted cell spreading, but also stimulated strong adhesive force and cell – cell contact, thus promoting tissue-like formation. However, the interplay of collagen with other ECM components such as fibronectin, laminin, and elastin is also valuable for the stable physiological functioning of hepatocytes. As a matter of fact, the differential effect on hepatocyte behavior has been studied in monolayer culture in previous studies [37–41]. For instance, fibronectin mediates its binding to integrins on the cell membrane and also binds to collagen on the ECM basal membrane. In other words, it may form a bridge between cells and collagen. This might provide an explanation for the reported enhanced spreading of hepatocytes on a fibronectin surface compared to that on a collagen surface [38]. In addition, fibronectin and collagen were confirmed to play distinct roles in the phenotypic regulation of cells cultured in a 3D environment in a report by Wang et al. [16]. Their results showed that, collagen-functionalized and fibronectin-functionalized inverted colloidal crystal (ICC) scaffold promoted albumin production and liver-specific gene expression compared to bare ICC scaffold.

Furthermore, we hypothesized that the functional expression of hepatocytes might also be stimulated by the residual or accumulated growth factors (GFs) on the L-ECM. Growth factors such as hepatocyte growth factor (HGF), fibroblast growth factor 2 (FGF-2), and epidermal growth factor (EGF) were shown to be present in the L-ECM after decellularization using ammonium hydroxide [42]. These GFs play a very important role in regeneration and proliferation of hepatocytes [43–45]. However, the quantities of these GFs may be vaguely preserved or completely denatured after pepsin treatment. Nevertheless, L-ECM is an organ-specific ECM with the ability to immobilize GFs [14], which may be directly attributed to the presence of GAGs. The GAG chains on the protein core are unbranched polysaccharide chains, composed of repetitive disaccharide units [4]. They are considered to have high electrostatic affinity with growth factors [46]. In a report by Ijima et al., hepatocyte-embedded L-ECM gel transplanted to partial hepatectomy treated rat obtained the largest aggregation and highest viability of transplanted hepatocytes [47]. Their results were directly linked to the immobilization of GFs such as HGF secreted by the partial hepatectomy treated rat on the L-ECM gel.

Based on the above results, the effectiveness of L-ECM II compared to L-ECM I may be concluded to be dependent on the concentration of L-ECM in 3D culture. However, in 2D culture, the hepatocyte tissue formed on L-ECM II was larger than that on L-ECM I. In other words, the composition of L-ECM II itself was shown to be superior over that of L-ECM I for hepatocyte culture. On the other hand, L-ECM I may be a good scaffold material as it also contains ECM molecules, however, may not be sufficient to fully supply the requirements of hepatocytes. The advantage of L-ECM II may also be attributed to the presence of balanced ECM molecules. As such, the relative abundance of each key molecule encourages suitable cell signals.

As we move towards the ultimate goal of clinical application, it is likely that more specialized scaffolds may be required to support various functional cell phenotypes. ECM biologic scaffolds have very significant characteristics and have opened up new perspectives for liver tissue reconstruction. In this study, though far from perfect, established a crucial step towards the development of L-ECM – based scaffolds. Our findings suggest that an intact L-ECM substrate can help maintain appropriate hepatocyte phenotype and suggest that an ECM from human liver could be similarly useful. However, to obtain a sufficient amount of human L-ECM is impossible. Thus, the availability of porcine L-ECM offers a meaningful advantage and more studies are expected to be done in the future. Finally, the use of human liver cells such as primary human hepatocytes is indispensable and could represent an ideal system for *in vitro* scaffold validation.

5. Conclusions

Influence of ECM proteins on the morphology and liver-specific functions of hepatocytes was confirmed in this study. L-ECM hydrogels produced by different methods exhibited different concentration of ECM proteins, especially collagen. L-ECM II hydrogel, with increased collagen concentration, resulted in improved biomechanical and viscoelastic properties. *In-vitro* 3D cultures showed higher relative expression of liver-specific functions (e.g.,

EROD activity, albumin production, and ammonia metabolism) in L-ECM II gel than in L-ECM I and I Col gels. Furthermore, in 2D culture, wider spread was observed in L-ECM II film, indicating a stronger cell-ECM interaction. These results of improved cell-ECM interactions have great implication for future studies involving primary hepatocytes, and might provide essential insights for the establishment of well-designed ECM-based substrates *in vitro*.

Conflicts of interest

The authors declare no conflict of interest.

Acknowledgments

The first author wishes to acknowledge the scholarship support by Engineering Research and Development for Technology (ERDT), Department of Science and Technology (DOST), Philippines.

Appendix A. Supplementary data

Supplementary data to this article can be found online at https://doi.org/10.1016/j.reth.2019.08.006.

References

[1] Theocharis AD, Skandalis SS, Gialeli C, Karamanos NK. Extracellular matrix structure. Adv Drug Deliv Rev 2016;97:4–27. https://doi.org/10.1016/j.addr.2015.11.001.
[2] Badylak SF. The extracellular matrix as a scaffold for tissue reconstruction. Semin Cell Dev Biol 2002;13:377–83. https://doi.org/10.1016/S1084.
[3] Freytes DO, Martin J, Velankar SS, Lee AS, Badylak SF. Preparation and rheological characterization of a gel form of the porcine urinary bladder matrix. Biomaterials 2008;29:1630–7. https://doi.org/10.1016/j.biomaterials.2007.12.014.
[4] Frantz C, Stewart KM, Weaver VM. The extracellular matrix at a glance. J Cell Sci 2010;123:4195–200. https://doi.org/10.1242/jcs.023820.
[5] Gilbert TW. Strategies for tissue and organ decellularization. J Cell Biochem 2012;113:2217–22. https://doi.org/10.1002/jcb.24130.
[6] Crapo PM, Gilbert TW, Badylak DVM. An overview of tissue and whole organ decellularization process. Biomaterials 2011;32:3233–43. https://doi.org/10.1016/j.biomaterials.2011.01.057.
[7] Sabetkish S, Kajbafzadeh AM, Sabetkish N, Khorramirouz R, Akbarzadeh A, Seyedian SL, et al. Whole-organ tissue engineering: decellularization and recellularization of three-dimensional matrix liver scaffolds. J Biomed Mater Res Part A 2015;103:1498–508. https://doi.org/10.1002/jbm.a.35291.
[8] Baptista PM, Siddiqui MM, Lozier G, Rodriguez SR, Atala A, Soker S. The use of whole organ decellularization for the generation of a vascularized liver organoid. Hepatology 2011;53:604–17. https://doi.org/10.1002/hep.24067.
[9] Wang Y, Nicolas CT, Chen HS, Ross JJ, De Lorenzo SB, Nyberg SL. Recent advances in decellularization and recellularization for tissue-engineered liver grafts. Cells Tissues Organs 2016;55901:1–12. https://doi.org/10.1159/000452761.
[10] Shirakigawa N, Takei T, Ijima H. Base structure consisting of an endothelialized vascular-tree network and hepatocytes for whole liver engineering. J Biosci Bioeng 2013;116:740–5. https://doi.org/10.1016/j.jbiosc.2013.05.020.
[11] Ijima H, Nakamura S, Bual R, Shirakigawa N, Tanoue S. Physical properties of the extracellular matrix of decellularized porcine liver. Gels 2018;4:1–15. https://doi.org/10.3390/gels4020039.
[12] Sellaro TL, Ranade A, Faulk DM, McCabe GP, Dorko K, Badylak SF, et al. Maintenance of human hepatocyte function in vitro by liver-derived extracellular matrix gels. Tissue Eng Part A 2010;16:1075–82. https://doi.org/10.1089/ten.TEA.2008.0587.
[13] Lee JS, Shin J, Park HM, Kim YG, Kim BG, Oh JW, et al. Liver extracellular matrix providing dual functions of two-dimensional substrate coating and three-dimensional injectable hydrogel platform for liver tissue engineering. Biomacromolecules 2014;15:206–18. https://doi.org/10.1021/bm4015039.
[14] Nakamura S, Ijima H. Solubilized matrix derived from decellularized liver as a growth factor-immobilizable scaffold for hepatocyte culture. J Biosci Bioeng 2013;116:746–53. https://doi.org/10.1016/j.jbiosc.2013.05.031.
[15] Bual R, Kimura H, Ikegami Y, Shirakigawa N, Ijima H. Fabrication of liver-derived extracellular matrix nanofibers and functional evaluation in in vitro culture using primary hepatocytes. Materialia 2018;4:518–28. https://doi.org/10.1016/j.mtla.2018.11.014.
[16] Wang Y, Kim MH, Shirahama H, Lee JH, Ng SS, Glenn JS, et al. ECM proteins in a microporous scaffold influence hepatocyte morphology, function, and gene expression. Sci Rep 2016;6:1–13. https://doi.org/10.1038/srep37427.
[17] Seglen PO. Chapter 4 preparation of isolated rat liver cells. Methods Cell Biol 1976;13:29–83. https://doi.org/10.1016/S0091-679X(08)61797-5.
[18] Ijima H, Kakeya Y. Monolayer culture of primary rat hepatocytes on an Arg-Gly-Asp (RGD)-immobilized polystyrene dish express liver-specific functions of albumin production and p-acetamidophenol metabolism the same as for spheroid culture. Biochem Eng J 2008;40:387–91. https://doi.org/10.1016/j.bej.2008.01.009.
[19] Lang R, Stern MM, Smith L, Liu Y, Bharadwaj S, Liu G, et al. Three-dimensional culture of hepatocytes on porcine liver tissue-derived extracellular matrix. Biomaterials 2011;32:7042–52. https://doi.org/10.1016/j.biomaterials.2011.06.005.
[20] Saheli M, Sepantafar M, Pournasr B, Farzaneh Z, Vosough M, Piryaei A, et al. Three-dimensional liver-derived extracellular matrix hydrogel promotes liver organoids function. J Cell Biochem 2018;119:4320–33. https://doi.org/10.1002/jcb.26622.
[21] Bual R, Kimura H, Ikegami Y, Shirakigawa N, Ijima H. Fabrication of liver-derived extracellular matrix nanofibers and functional evaluation in in vitro culture using primary hepatocytes. Materialia 2018;4C:518–28. https://doi.org/10.1016/J.MTLA.2018.11.014.
[22] Sato K, Ebihara T, Adachi E, Kawashima S, Hattori S, Irie S. Possible involvement of aminotelopeptide in self-assembly and thermal stability of collagen I as revealed by its removal with proteases. J Biol Chem 2000;275:25870–5. https://doi.org/10.1074/jbc.M003700200.
[23] Brown B, Lindberg K, Reing J, Stolz DB, Badylak SF. The basement membrane component of biologic scaffolds derived from extracellular matrix. Tissue Eng 2006;12:519–26. https://doi.org/10.1089/ten.2006.12.519.
[24] Shoulder RTR MD. Collagen structure and stability. Annu Rev Biochem 2009:929–58. https://doi.org/10.1146/annurev.biochem.77.032207.120833 [COLLAGEN].
[25] Yu H, Mouw JK, Weaver VM. Forcing form and function: biomechanical regulation of tumor evolution. Trends Cell Biol 2011;21:47–56. https://doi.org/10.1016/j.tcb.2010.08.015. Forcing.
[26] Lu P, Takai K, Weaver VM, Werb Z. Extracellular Matrix degradation and remodeling in development and disease. Cold Spring Harb Perspect Biol 2011;3:1–24. https://doi.org/10.1101/cshperspect.a005058.
[27] Daley WP, Peters SB, Larsen M. Extracellular matrix dynamics in development and regenerative medicine. J Cell Sci 2008;121:255–64. https://doi.org/10.1242/jcs.006064.
[28] Wells RG. The role of matrix stiffness in regulating cell behavior. Hepatology 2008;47:1394–400. https://doi.org/10.1002/hep.22193.
[29] Kular JK, Basu S, Sharma RI. The extracellular matrix: structure, composition, age-related differences, tools for analysis and applications for tissue engineering. J Tissue Eng 2014;5:1–17. https://doi.org/10.1177/2041731414557112.
[30] Le Thi P, Lee Y, Nguyen DH, Park KD. In situ forming gelatin hydrogels by dual-enzymatic cross-linking for enhanced tissue adhesiveness. J Mater Chem B 2017;5:757–64. https://doi.org/10.1039/c6tb02179d.
[31] Meyvis TKL, De Smedt SC, Demeester J, Hennink WE. Influence of the degradation mechanism of hydrogels on their elastic and swelling properties during degradation. Macromolecules 2000;33:4717–25. https://doi.org/10.1021/ma992131u.
[32] Kharkar PM, Kiick KL, Kloxin AM. Designing degradable hydrogels for orthogonal control of cell microenvironments. Chem Soc Rev 2013;42:7335–72. https://doi.org/10.1039/c3cs60040h.
[33] Lin CC, Anseth KS. PEG hydrogels for the controlled release of biomolecules in regenerative medicine. Pharm Res 2009;26:631–43. https://doi.org/10.1007/s11095-008-9801-2.
[34] Tibbitt MW, Anseth KS. Hydrogels as extracellular matrix mimics for 3D cell culture. Biotechnol Bioeng 2009;103:655–63. https://doi.org/10.1002/bit.22361.
[35] Yamamoto J, Udono M, Miura S, Sekiya S, Suzuki A. Cell aggregation culture induces functional differentiation of induced hepatocyte-like cells through activation of Hippo signaling. Cell Rep 2018;25:183–98. https://doi.org/10.1016/j.celrep.2018.09.010.
[36] Stamenkovic I. Extracellular matrix remodelling: the role of matrix metalloproteinases. J Pathol 2003;200:448–64. https://doi.org/10.1002/path.1400.
[37] Rubin K, Staffan J, Hook M, Obrink B. Substrate adhesion OF rat hepatocytes: on the role of fibronectin in cell spreading. Exp Cell Res 1981;135:127–35.
[38] Sánchez A, Álvarez AM, Pagan R, Roncero C, Vilaró S, Benito M, et al. Fibronectin regulates morphology, cell organization and gene expression of rat fetal hepatocytes in primary culture. J Hepatol 2000;32:242–50. https://doi.org/10.1016/S0168-8278(00)80069-0.
[39] Sawada N, Tomomura A, Sattler CA, Sattler GL, Kleinman HK, Pitot HC. Effects of extracellular matrix components on the growth and differentiation of cultured rat hepatocytes. In Vitro Cell Dev Biol 1987;23:267–73. https://doi.org/10.1007/BF02623709.
[40] Johansson S, Hook M. Substrate adhesion of rat hepatocytes: mechanism of attachment to collagen substrates. J Cell Biol 1984;98:810–7. https://doi.org/10.1083/jcb.98.3.810.
[41] Sawada N, Tomomura A, Sattlet A, Sattler GL, Kleinman HK, Pitot HC. Extracellular matrix components influence DNA synthesis of rat hepatocytes in primary. Culture 1986;167:458–70.
[42] Coronado RE, Somaraki-Cormier M, Natesan S, Christy RJ, Ong JL, Halff GA. Decellularization and solubilization of porcine liver for use as a substrate for

porcine hepatocyte culture. Cell Transplant 2017;26:1840–54. https://doi.org/10.1177/0963689717742157.
[43] Hammond JS, Gilbert TW, Howard D, Zaitoun A, Michalopoulos G, Shakesheff KM, et al. Scaffolds containing growth factors and extracellular matrix induce hepatocyte proliferation and cell migration in normal and regenerating rat liver. J Hepatol 2011;54:279–87. https://doi.org/10.1016/j.jhep.2010.06.040.
[44] Hou Y Te, Ijima H, Takei T, Kawakami K. Growth factor/heparin-immobilized collagen gel system enhances viability of transplanted hepatocytes and induces angiogenesis. J Biosci Bioeng 2011;112:265–72. https://doi.org/10.1016/j.jbiosc.2011.05.003.
[45] Whitaker MJ, Quirk RA, Howdle SM, Shakesheff KM. Growth factor release from tissue engineering scaffolds. J Pharm Pharmacol 2001;53:1427–37. https://doi.org/10.1211/0022357011777963.
[46] Michalopoulos GK, Zarnegar R. Hepatocyte growth factor. Hepatology 1992;15:149–55. https://doi.org/10.1002/hep.1840150125.
[47] Ijima H, Nakamura S, Bual RP, Yoshida K. Liver-specific extracellular matrix hydrogel promotes liver-specific functions of hepatocytes in vitro and survival of transplanted hepatocytes in vivo. J Biosci Bioeng 2019. https://doi.org/10.1016/j.jbiosc.2019.02.014.